

Self-trapping at the liquid-vapor critical point: A path-integral study

Bruce N. Miller*

Department of Physics and Astronomy, Texas Christian University, Fort Worth, Texas 76129, USA

Terrence L. Reese

Department of Physics, Southern University and A&M College, Baton Rouge, Louisiana 70813, USA

(Received 17 June 2008; published 23 December 2008)

Experiments suggest that localization via self-trapping plays a dominant role in the behavior of a low-mass particle, e.g., an electron, positron, or positronium atom, in both liquids and supercritical fluids. In the latter case, the behavior is dominated by the liquid-vapor critical point. However, because of its large isothermal compressibility, the critical point is difficult to probe both experimentally and theoretically. Here we present the results of path-integral computations of the characteristics of a generic self-trapped particle at the critical point of a Lennard-Jones fluid for a positive particle-atom scattering length. We carefully investigate the dependence of the properties of both the self-trapped quantum particle and the proximal fluid on the range of the direct particle-atom interaction. To the extent that the generic particle mimics the behavior of ortho-positronium, qualitative information is provided on the pick-off decay rate. In general, compared with self-trapping at higher temperature, we find that the localized quantum defect has a much larger range of influence on the host fluid. In particular, it appears that long-range density oscillations are induced in the fluid surrounding the defect. The results also suggest that, even at the critical point, there is a minimum interaction range below which self-trapping does not occur.

DOI: [10.1103/PhysRevE.78.061123](https://doi.org/10.1103/PhysRevE.78.061123)

PACS number(s): 64.60.-i, 05.70.Jk

I. INTRODUCTION

Starting with the work of Einstein [1], the system consisting of a massive particle equilibrated in a host fluid, known to physicists and chemists as Brownian motion, has played a seminal role in the development of statistical physics. However, the opposite regime of an equilibrated low-mass particle is equally challenging and manifests a richer set of behaviors. Except at very high temperatures, quantum mechanics is required to model the low mass particle. Possible quantum particle (QP) candidates are an electron, positron, or positronium atom, while the host can be either a dense gas or liquid below the critical temperature, or a supercritical fluid above it. Experimental measurements of the properties of a low-mass particle equilibrated in a fluid strongly suggest that it can induce a local deformation in the fluid in which the QP becomes self-trapped, or localized [2,3]. Since the QP has a long de Broglie wavelength, intuitively we anticipate that it simultaneously interacts with a large group of atoms or molecules in the host fluid, forming a mesoscopic region of altered fluid density. Depending on whether the effective QP-atom interaction is attractive or repulsive, the local density of the host is either augmented or suppressed near the QP, resulting in the formation of either a “microdroplet” or a “microbubble.” The intuitive picture is completed by imagining that the QP occupies the ground state of the potential well induced by the formation of the density inhomogeneity, i.e., the droplet or bubble, thus stabilizing the deformation.

Since the positron always has a negative scattering length, the experimental manifestation of self-trapping is a sharp de-

crease in the positron lifetime due to the increase in the local electron density resulting from the formation of a droplet. The reverse is true for ortho-positronium: Angular momentum conservation eliminates the two photon decay process for o-Ps so its natural lifetime in the vacuum is about 140 ns [2]. However, its positron can annihilate more easily with a host electron. A consequence of the fermionic repulsion between the electron in o-Ps and the electrons of the host fluid is that this “pick-off” annihilation rate is reduced when self-trapping occurs, demonstrating bubble formation [2]. Depending on the host, the electron-atom scattering length can have either sign, so both behaviors are possible. While the most dramatic manifestation of self-trapping of the positron or positronium is a change in lifetime, the fingerprint of electron self-trapping is a change in mobility [4].

In addition to the liquid state [5,6], self-trapping occurs in a broad region of density ρ and temperature T surrounding the liquid-vapor critical point (ρ_c, T_c) [7]. Since the isothermal compressibility diverges at the critical point [8], this is not surprising: The QP can more easily alter the local density in this region of temperature and density. However, as a result of the large density gradient induced by the earth’s gravitational field, there are few reliable experimental studies of self-trapping close to the critical point [9,10]. Thus, although it dominates the self-trapping regime above T_c , the effect of close proximity to this point on self-trapping is not generally known [9,10].

The theory of self-trapping has evolved through different stages: In the earliest models, the QP simply sits in the ground state of a spherical step potential which is assumed to be proportional to the local fluid density [11]. In modeling the QP-host interaction the atomic nature of the host is ignored, and it is represented by a type of jellium. By minimizing the free energy of the QP-fluid system, it is possible to show that the deformation is stable in a bounded region of

*b.miller@tcu.edu

temperature and density near the critical point [11]. Later versions of mean field theory (MFT) permitted a continuous density profile [7,12] and took into account the atomic nature of the host at an intermediate level [13]. An interesting improvement was obtained by including the effect of correlations between the fluid atoms via the Percus-Yevick equation [14]. An advantage of MFT is that computations are reduced to numerical integration of a pair of coupled ordinary differential equations. However, in practice, they have proved useful only for fluids at low temperatures [7,12,14,15]. This problem may arise because mean field theories include only a single bound state for the QP. This approach was complemented by the work of Hernandez, who carefully considered the role of the QP density of states [3].

More microscopically complete models have evolved during the last few decades based on the Feynman-Kac path integral [16], which overcome a number of shortcomings of the earlier work. These account for the details of the QP-fluid interaction, and also take into account local fluctuations in the disturbed fluid. Three general approaches have been used, analytic methods that couple the density functional theory of complex fluids with the Fourier representation of the path integral [17–19], the more direct alternative employing Monte Carlo algorithms [20,21] and the application of molecular dynamics to the equivalent classical system [22,23]. For reviews see [24,25]. While the latter two avoid approximation, the computational cost is higher. The first two approaches have been employed to examine the self-trapping of electrons, positrons, and positronium in supercritical xenon [15,26–31].

Here we employ the path integral Monte Carlo (PIMC) technique to investigate self-trapping of a generic quantum particle at the liquid-vapor critical point. Improvements in fluid equilibrium theory provide accurate critical point parameters for the Lennard-Jones 6-12 potential in both the truncated and continuous versions [32,33]. We take advantage of these results in selecting the values of the Lennard-Jones parameters that correspond to the correct critical density and temperature. Using the PIMC technique, we model the QP-atom interaction with a hard-sphere potential and study the dependence of the physical and statistical properties of self-trapping on the hard sphere diameter R_{HS} at the liquid-vapor critical point. In particular, we investigate the dependence on R_{HS} of the spreading of the QP wave function, and the behavior of the QP-atom correlation function and the local density of fluid atoms surrounding the average QP center of mass. Since a repulsive QP-atom interaction is approximately representative of positronium [2], we also estimate the pick-off annihilation rate for a simplified model of the atomic charge distribution.

Although, for reasons given above, no experimental measurements of the pick-off decay rate have been carried out precisely at the critical point, for the case of xenon they exist for two supercritical temperatures (300 and 340 K) over a large density range, and strongly suggest the existence of the Ps self-trapped state [34]. In previous work, we have used the PIMC method and the reference interaction site model (RISM) polaron theory to carry out simulations of both e^+ [27,29] and Ps in xenon [26,30] at these temperatures, so it is natural to select the critical point of xenon as a test case. The

truncated version of the Lennard-Jones (LJ) 6-12 potential was chosen to represent the interatomic potential because Wilding has established numerically accurate connections between the LJ distance and energy parameters (σ and ε) and the critical temperature and density (T_c and ρ_c) [32]. In the following we chose values of σ and ε and the QP mass, m , suitable for positronium equilibrated in xenon.

The paper is organized as follows. In Sec. II we explain the path-integral formulation of the system, the potentials that were selected to approximate the QP-atom and interatomic interactions, the computational methods employed, and the important structural quantities that characterize the localized QP such as the QP-atom radial distribution function, and how they determine the decay rate [21]. In Sec. III the results from the PIMC calculations are examined. In a preliminary study, we considered the same system with a fixed size and number of fluid atoms for three values of the hard sphere diameter [35,36]. Here, in this expanded investigation, we obtain the dependence of the mean values on the hard sphere diameter from 0.5 to 9.5 Å in 0.5 Å increments. Furthermore, we consider the convergence of the mean values in terms of the size of the number of imaginary time slices [24], the system size, and the total number of trials. In Sec. IV we present our conclusions and suggestions for future investigations.

II. PATH-INTEGRAL MONTE CARLO TECHNIQUE

A. Hybrid model

Except at very low temperatures, the translational degrees of freedom of an atomic fluid can be approximated with classical mechanics. Thus the energy of the QP-fluid system is well represented by a hybrid classical-quantum Hamiltonian:

$$H = \sum_1^N \mathbf{P}_j^2/2M + \sum_{N \geq j > k \geq 1} U(|\mathbf{R}_j - \mathbf{R}_k|) + H_{\text{QP}}, \quad (1)$$

where

$$H_{\text{QP}} = -\frac{\hbar^2}{2m} \Delta + \sum_1^N V(|\mathbf{r} - \mathbf{R}_j|). \quad (2)$$

Here \mathbf{P}_j and \mathbf{R}_j are the momenta and positions of the N host atoms, \mathbf{r} is the position of the QP, and U and V are the pairwise additive atom-atom and QP-atom interaction potentials. This is known as the adiabatic approximation and results in a hybrid partition function [30]

$$Z = \int d\mathbf{R} e^{-\beta U(\mathbf{R})} \int d\mathbf{r} \langle \mathbf{r} | e^{-\beta H_{\text{QP}}} | \mathbf{r} \rangle / (N! \Lambda^{3N}), \quad (3)$$

where here \mathbf{R} represents the complete $3N$ -dimensional configuration space of the atoms with classical potential energy $U(\mathbf{R})$, and Λ is the atomic thermal wavelength. Thus, in principle, the quantum statistical average of the physical operator $\hat{\mathcal{O}}$ can be computed from

$$\langle \hat{\mathcal{O}} \rangle = \int d\mathbf{R} e^{-\beta U(\mathbf{R})} \int d\mathbf{r} \langle \mathbf{r} | e^{-\beta H_{\text{QP}}} \hat{\mathcal{O}} | \mathbf{r} \rangle / (N! \Lambda^{3N} Z). \quad (4)$$

To obtain a formulation that is useful for computation, we follow the Feynman-Kac path-integral construction [16]. First, by applying the Trotter formula to the quantum part of Z ,

$$e^{-\beta H_{\text{PQ}}} = (e^{-\beta H_{\text{PQ}}/P})^P, \quad (5)$$

we can express the trace over \mathbf{r} as a sum over discretized paths of P steps,

$$\int d\mathbf{r} \langle \mathbf{r} | e^{-\beta H_{\text{QP}}} | \mathbf{r} \rangle = \prod_{i=0}^{P-1} \int d\mathbf{r}_i \langle \mathbf{r}_i | e^{-\beta H_{\text{QP}}/P} | \mathbf{r}_{i+1} \rangle, \quad (6)$$

where $\mathbf{r} = \mathbf{r}_0 = \mathbf{r}_P$. Each \mathbf{r}_i represents a different position for the particle at a different imaginary time slice. For sufficiently large P , the kinetic and potential energy operators approximately commute in each step, yielding the following expression for the partition function [16]:

$$Z_P = \int d\mathbf{R} e^{-\beta U(\mathbf{R})} \left(\prod_{i=0}^{P-1} \int d\mathbf{r}_i \mathbf{Q}_i(\mathbf{r}_i, \mathbf{r}_{i+1}, \mathbf{R}, \beta) \right), \quad (7)$$

where

$$\begin{aligned} \mathbf{Q}_i(\mathbf{r}_i, \mathbf{r}_{i+1}, \mathbf{R}, \beta) &= \langle \mathbf{r}_i | e^{-\beta H_{\text{QP}}/P} | \mathbf{r}_{i+1} \rangle \\ &= e^{-P|\mathbf{r}_i - \mathbf{r}_{i+1}|^2/2\lambda^2} \vartheta(\mathbf{r}_i, \mathbf{r}_{i+1}, \mathbf{R}; \beta/P). \end{aligned} \quad (8)$$

$\sqrt{2\pi}\lambda$ is the QP thermal wavelength and ϑ is the density matrix contribution arising from the interaction between the particle and the fluid. In the limit $P \rightarrow \infty$, $Z_P \rightarrow Z$. This is the discretized path-integral formulation and is equivalent to a closed chain of P classical particles equilibrated in a fluid at the augmented temperature $(P/k\beta)$ [20,37]. This equivalence is known as the classical isomorphism and it is important because it allows Monte Carlo methods developed for classical systems to be used to compute quantum mechanical equilibrium values. The spread of the chain corresponds to the mean quantum spread of the QP wave function. If we take ϑ to be equal to $\exp(-\beta V/P)$, Eq. (8) is known as the primitive approximation. The path-integral Monte Carlo method has been used successfully by a number of groups, including our own, to compute the equilibrium properties of quantum systems [15,29,30,38].

B. Polymer-fluid interaction potential

The interaction between the QP and the fluid is vested in ϑ , whose form depends on the type of approximation used to represent the interaction between the QP and the fluid atoms or molecules. In the primitive approximation ϑ is represented by $\exp(-\beta \sum_{i,j} V(|\mathbf{r}_i - \mathbf{R}_j|))/P$, where $|\mathbf{r}_i - \mathbf{R}_j|$ is the distance between the i th polymer particle and the j th fluid molecule. To provide a good representation of the strong, short-range, fermionic repulsion between the electron of the Ps atom and the electrons of the fluid molecules, in our previous calculations we used the hard sphere interaction to simulate Ps in xenon. The interaction has one parameter, the hard sphere diameter (R_{HS}), which is the minimum distance that can occur between the centers of a polymer particle and a fluid molecule. If the distance between the center of a poly-

mer particle and a fluid molecule, $|\mathbf{r}_i - \mathbf{R}_j|$, is less than R_{HS} then the interaction potential becomes infinite, making this an unacceptable configuration [$\vartheta=0, V(|\mathbf{r}_i - \mathbf{R}_j|)=\infty$]. In the primitive approximation, when the distance is greater than R_{HS} then the potential is zero and the configuration is acceptable [$\vartheta=1, V(|\mathbf{r}_i - \mathbf{R}_j|)=0$].

The path-integral formulation is known to be accurate only if the interaction potential changes slowly over distances on the order of the separation between adjacent polymer particles. Thus, the greater the gradient of the potential, the more classical pseudoparticles (or imaginary time slices) needed to accurately simulate the polymer-fluid interaction potential. Because the hard sphere potential is discontinuous at R_{HS} , in principle an infinite number of particles are required to satisfy this condition at the hard sphere boundary. In practice, convergence can be obtained but requires a large value of P and the convergence is very slow. An impressive reduction in the value of P can be obtained by replacing the strict hard sphere potential with the image approximation [39]. It represents the discontinuity as a rapidly decreasing but continuous exponential function. In our computations we use the function devised by Whitlock and Kalos [40]. This approximation sets the density matrix equal to zero when $|\mathbf{r}_i - \mathbf{R}_j|$ or $|\mathbf{r}_{i+1} - \mathbf{R}_j| < R_{\text{HS}}$ and

$$\vartheta(\mathbf{r}_i, \mathbf{r}_{i+1}, \mathbf{R}_j; \beta/P) = 1 - \exp[-2PF(\mathbf{r}_i, \mathbf{r}_{i+1}, \mathbf{R}_j)/(\lambda R_{\text{HS}})^2], \quad (9)$$

where

$$F(\mathbf{r}_i, \mathbf{r}_{i+1}, \mathbf{R}_j) = (|\mathbf{r}_i - \mathbf{R}_j|^2 - R_{\text{HS}}^2)(|\mathbf{r}_{i+1} - \mathbf{R}_j|^2 - R_{\text{HS}}^2) \quad (10)$$

when both $|\mathbf{r}_i - \mathbf{R}_j|$ and $|\mathbf{r}_{i+1} - \mathbf{R}_j| \geq R_{\text{HS}}$. The gradient of ϑ with respect to \mathbf{R}_j , calculated from Eq. (9), just beyond R_{HS} is sufficiently large to approximate the hard sphere potential at the discontinuity and yet result in reasonable values of P . Alternatively, rapid convergence could also have been obtained by the scattering approach for approximating the imaginary time propagator introduced by Storer [41,42] and applied to the hard sphere interaction by Cao and Berne [43].

C. Fluid-fluid interaction potential

The truncated version of the Lennard-Jones 6-12 potential,

$$U(R') = 4\epsilon[(\sigma/R')^{12} - (\sigma/R')^6], \quad (11)$$

where $R' = |\mathbf{R}_i - \mathbf{R}_j|$ and σ and ϵ are the LJ distance and energy parameters, respectively, was chosen to represent the interaction potential between the fluid atoms. In the truncated version $U(R')$ is computed only when $R' < 2.5\sigma$. Otherwise it is defined as zero. Using finite-size-scaling techniques, Wilding has established numerically accurate connections between σ and ϵ and the critical temperature and density (T_c and ρ_c), namely, $\rho_c^* = \rho_c \sigma^3 = 0.3197$ and $kT_c/\epsilon = 1.1876$ [32]. Since experimental values of the o-Ps pick-off decay rate have been measured over a wide density range not too far from the critical temperature, we chose values of σ and ϵ suitable for positronium equilibrated in xenon. The experi-

mentally measured values of the critical temperature and density of xenon are given in the literature as $T_c=289$ K and $\rho_c=5.299 \times 10^{-3}$ atoms/Å³, thus yielding $\sigma=3.92$ Å and $\varepsilon/k=243.5$ K.

D. Computational methods

The most common Monte Carlo method used in statistical simulations of equilibrium is the Metropolis sampling algorithm (MSA) [44]. The standard MSA creates new configurations for each particle of the system separately by moving the particle a random distance from its initial point and re-computing the system's energy in this trial configuration. If the ratio of the Boltzmann weight of the trial configuration to the original configuration is less than a random number between zero and one, then the trial position is accepted and it replaces the original. If not, then the trial position is rejected and the original position for this particle is kept. After an attempted movement has been made for each particle in the system, which is our definition of a pass, the equilibrium properties of the system are computed. A large enough number of passes must be carried out to ensure the convergence of the average values. In our algorithm the standard MSA is used to compute the average of the equilibrium properties of the fluid. However, because of the unique convergence issues involved with the polymer, sequential trial movements of the particles on the chain do not sufficiently explore its configuration space. The most efficient way of sampling different configurations for the chain would be to create a new configuration of the complete chain for each pass. However, this results in a high degree of failed configurations in which the interaction potential energy is too high. As a compromise between, on the one hand, moving the entire chain or, on the other, moving particles one at a time, trial positions for the polymer particles can be created on a subchain consisting of n particles. A balance must be struck in which a large enough number of particles on the subchain are moved to ensure that the phase space is adequately explored, yet not so many that a majority of attempted configurations is rejected. In test computations it was determined that an effective value of n was 10% of the total number of particles on the chain [20].

E. Important quantities

1. Structural quantities

The important quantities characterizing the QP-fluid system fall into two categories, those directly indicating how the fluid is affected by the QP and, conversely, those that show how the fluid affects the QP. We chose to examine two quantities in each group. The polymer-fluid radial distribution function $g_{\text{PF}}(r)$ and the density of fluid molecules a distance r from the polymer center of mass, $g_{\text{fc.m.}}(r)$, are the quantities structurally related to how the QP affects the fluid. The function $g_{\text{PF}}(r)$ is the average density of fluid molecules at a distance r from the polymer particles and is normalized to 1 at large distances. It is represented by the expression

$$g_{\text{PF}}(r) = \left\langle \sum_{i=0}^{P-1} \sum_{j=1}^N \delta(\mathbf{r}_i - \mathbf{R}_j - \mathbf{r}) \right\rangle / (\rho P), \quad (12)$$

where ρ is the average molecular number density and \mathbf{r} is the displacement between the i th polymer particle and the j th

fluid molecule. Due to homogeneity and isotropy, g_{PF} only depends on r . In an extended state, the polymer chain is spread out over a distance scale of order λ , and the density of fluid molecules just beyond R_{HS} should be nearly equal to the average density. However, in a self-trapped state, the polymer chain becomes wrapped in such a tight arrangement that some of the particles become confined to the internal portion of the chain configuration, and the fluid molecules cannot penetrate the cluster of these segregated particles as they can those on the outside of the chain. Thus, in a plot of g_{PF} versus position, the g_{PF} curve increases toward the average density much more slowly than that for an extended state.

The density of fluid molecules measured from the polymer center of mass can be used to directly determine whether a self-trapped state exists. It is given by

$$g_{\text{fc.m.}}(r) = \left\langle \sum_{j=1}^N \delta(\mathbf{R}_j - \mathbf{r}_{\text{c.m.}} - \mathbf{r}) \right\rangle / \rho \quad (13)$$

where $\mathbf{r}_{\text{c.m.}}$ is the position of the polymer center of mass. In an extended state, fluid atoms are able to penetrate into the vicinity of the chain c.m. because it is relatively spread out. On the other hand, in a completely self-trapped state, ground state dominance prevails, the chain is folded upon itself within the volume of the bubble, and fluid atoms are totally expelled from this region.

There are also two convenient structural quantities that explore how the polymer chain is affected by the fluid. The root mean square displacement between two particles on the chain, $D(|t-t'|)$, is

$$D(t' - t) = \sqrt{\langle |\mathbf{r}(t) - \mathbf{r}(t')|^2 \rangle}, \quad (14)$$

where t labels the time slice, or polymer pseudoparticle, along the chain. Like $g_{\text{fc.m.}}$, this quantity directly indicates the existence of a self-trapped state. In an extended state the polymer is spread out so that $D(|t-t'|)$ increases with respect to $|t-t'|$ until the halfway point of the chain ($|t-t'|=P/2$), where it achieves its maximum value. In a self-trapped state the polymer chain folds up on itself so that the displacement between particles t and t' becomes constant except near the end points ($|t-t'|=0$ or P). Another measure of the effect of the fluid on the polymer is measured by the mean density of polymer particles from the polymer c.m. $g_{\text{pc.m.}}(r)$. In a self-trapped state most of the pseudoparticles become confined to the vicinity of the c.m., in contrast with an extended state where a higher percentage of the particles are able to spread out much further from the c.m. The density of polymer particles from the c.m. is given by

$$g_{\text{pc.m.}}(r) = \left\langle \sum_{i=0}^{P-1} \delta(\mathbf{r}_i - \mathbf{r}_{\text{c.m.}} - \mathbf{r}) \right\rangle \quad (15)$$

and is proportional to the mean square of the QP wave function. The final structural quantity is the fluid intermolecular radial distribution function:

$$g_{ff}(r) = \left\langle \sum_{i>j=1}^N \delta(\mathbf{R}_i - \mathbf{R}_j - \mathbf{r}) \right\rangle / (\rho N), \quad (16)$$

which measures the average density of fluid molecules from each other. Although a different approach was employed here, because of the uniqueness of the g_{ff} plot at the critical point, in principle it can be used to determine whether the fluid is at the critical point. A more detailed discussion of these quantities and how they are computed can be found in our previous paper on the self-trapping of Ps in xenon [30].

2. Decay rate

Because the positron annihilates with an electron belonging to one of the fluid molecules, the pick-off decay rate depends directly upon the local molecular density near the Ps atom. Unlike the structural quantities mentioned above, this is the property of the system that is measured in experiments. The formation of a self-trapped state around the Ps atom results in a decrease in the density of electrons available for annihilation. The decay rate observable can be represented by the operator

$$\hat{\lambda} = \sum_{j=1}^N f(|\mathbf{R}_j - \mathbf{x}_+|), \quad (17)$$

where $f(|\mathbf{R}_j - \mathbf{x}_+|)$ is the electron density contributed by the j th atom at the position of the positron (\mathbf{x}_+). Since we are interested in temperatures well below the excitation energy of positronium, we assume that it remains in the ground state until annihilation occurs, in which case the Ps wave function separates into the product $\varphi_0(\mathbf{x}_{\text{rel}})\psi(\mathbf{x}_{\text{c.m.}})$ where $\mathbf{x}_{\text{c.m.}} = (\mathbf{x}_+ + \mathbf{x}_-)/2$ is the center of mass of the Ps atom, and $\mathbf{x}_{\text{rel}} = \mathbf{r}_+ - \mathbf{r}_-$ is the vector displacement between the positron and the electron. Then, fixing the molecular positions, the conditional average of $\hat{\lambda}$ in the adiabatic representation is

$$\langle \psi | \hat{\lambda} | \psi \rangle = \int \int \sum_1^N f(|\mathbf{R}_j - \mathbf{x}_{\text{c.m.}} - \mathbf{x}_{\text{rel}}/2|) \times |\varphi_0(\mathbf{x}_{\text{rel}})|^2 |\psi(\mathbf{x}_{\text{c.m.}})|^2 d\mathbf{x}_{\text{c.m.}} d\mathbf{x}_{\text{rel}}, \quad (18)$$

where we have transformed the integral to the relative and center of mass coordinates. The hydrogenic ground state wave function for the relative coordinate is simply proportional to $\exp(-x_{\text{rel}}/2a_0)$. To apply the Feynman-Kac formulation to positronium, we treat it as a composite particle with translational coordinate $\mathbf{x}_{\text{c.m.}}$. Then, in the adiabatic representation, the center of mass density is represented by a sum of δ functions centered at the time slices \mathbf{r}_i of the discretized path integral [see Eq. (15)].

Here our goal is to obtain useful qualitative information concerning the behavior of the dependence of the mean decay rate on the positronium-molecule interaction at the critical point. Then, for simplicity, we will assume that the electrons available for pick-off annihilation are concentrated at the molecular positions, i.e., $f(|\mathbf{R}_j - \mathbf{x}_+|) \sim \delta(\mathbf{R}_j - \mathbf{x}_+)$. With these assumptions, the conditional quantum average is easily reduced to

$$\langle \psi | \hat{\lambda} | \psi \rangle = \frac{1}{\pi a_0^2 P} \sum_{i,j} \exp\left(-\frac{2}{a_0} |\mathbf{R}_j - \mathbf{r}_i|\right). \quad (19)$$

Using the weights of the discretized path integral to average over time slices and molecular positions quickly yields

$$\bar{\lambda} = \frac{\rho}{\pi a_0^2} \int d\mathbf{r} \exp(-2r/a_0) g_{\text{PF}}(r) \quad (20)$$

for the mean decay rate modulo a normalization factor. Thus the pick-off decay rate is determined by the distribution of fluid atoms in the neighborhood of the chain pseudoparticles. The existence of a stable localized QP will depress the value of $g_{\text{PF}}(r)$ and, consequently, the value of the decay rate. The pick-off decay rate is the property that is actually measured in experiments examining the self-trapping of positronium [30].

III. RESULTS

A. Convergence

An important factor in PIMC computations is the issue of convergence, assuring that the computed equilibrium values of the system do not change significantly when the system size (the number of fluid molecules N), the number of pseudoparticles P , and the number of statistical samples (passes) are increased. To accomplish this we simply increased all three parameters while maintaining a constant temperature and average fluid density until there was no significant change in the results. From previous test runs, the number of polymer particles required for convergence was found to be dependent upon the density and temperature. A value of $P=2000$ was found to be more than adequate for densities greater than ρ_c^* . Since most of the CPU time was expended on repositioning the atoms, this large value of P did not pose a problem and helped ensure convergence. The number of samples was found to be only weakly dependent upon the system characteristics, with at least several thousand required for convergence.

The number of fluid atoms is related to the volume in which the system resides. In our previous calculations we assumed the volume to be a cube, and our initial assumption was that the sides should be three times the length of the QP thermal wavelength to minimize size effects. The positions of the fluid atoms were distributed based on periodic boundary conditions. While this assumption worked fairly well for our simulations in xenon at $T=300$ and 340 K, the large isothermal compressibility at the critical point may require a larger volume so that the fluid molecules are not forced to crowd upon each other at the edge of the cube (simulations were always initiated with the chain c.m. at the cube center). This possibility was investigated at the critical point using test runs computing the pick-off decay rate at different values of N . The minimum value of N was calculated as before using the critical density ($\rho_c^*=0.319$) and assuming a cube with sides of length three times the thermal wavelength, $3\sqrt{2}\pi\lambda$, resulting in a value of $N=4254$. We computed the decay rate using both $N=4254$ and 8500 to test the convergence with respect to N . The percent difference between

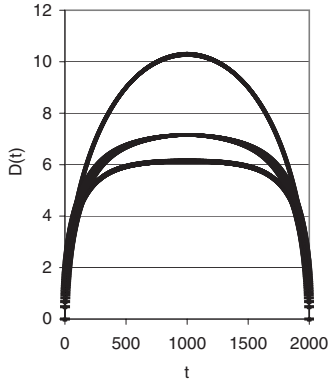


FIG. 1. Root mean square displacement D (\AA) versus the number of imaginary time links ($t-t'$) along the chain for three values of the QP-atom interaction range R_{HS} ; 0.5 (top line), 5.0 (middle line), and 9.5 \AA (bottom line).

these results was 2.24, indicating that near the liquid-vapor critical point the system size needs to be increased to account for the impact of the long-range intermolecular correlations. Computations were again carried out using a value of $N = 10\,000$, which resulted in a percent difference of only 0.95 as compared to the decay rate computed at $N = 8500$. We also tested the accuracy of the algorithm by carrying out the simulations at a very small R_{HS} . This reduces the self-trapping effect, which should result in a pick-off decay rate equal to the average density ($\rho_c^* = 0.3190$). These computations were carried out at an R_{HS} of 0.005 \AA for $N = 4254$, 8500, and 10 000. The calculated decay rates were 0.309, 0.316, and 0.321, resulting in percent errors of 3.1, 0.9, and 0.6, respectively, showing that at the liquid-vapor critical point edge effects significantly affect the calculations. The issue of size effects as it relates to structural quantities will be discussed in more detail in the next section.

B. Structural results

Here we report on the results of path-integral simulations over the range $0.5 < R_{\text{HS}} < 9.5$ \AA in 0.5 \AA increments. Two important characteristics of the QP are the root mean square displacement D between two particles along the chain, and the density of chain particles from the chain center of mass $g_{\text{pc.m.}}(r)$. As mentioned earlier, both D and $g_{\text{pc.m.}}(r)$ provide direct measures of self-trapping. Figure 1 is a plot of D versus $|t-t'|$ for three values of R_{HS} stated above. The upper curve has a parabolic shape that would be expected for an extended state. In fact, for small R_{HS} , the shape of the curve is very close to that of a free particle, one where there are no fluid molecules. As R_{HS} increases, the figure shows that the shape of the plots changes from parabolic, corresponding to a nearly free particle, to one that is essentially constant in the central region, indicating that the chain has become more confined [20,37]. The strength of trapping can be related to the length over which D is constant. The longer this region, the more deeply the QP is trapped in the effective potential well. Increasing the value of R_{HS} expels fluid atoms from the vicinity of the chain particles. At the same time, the pressure applied by the fluid atoms compresses the chain. Since there

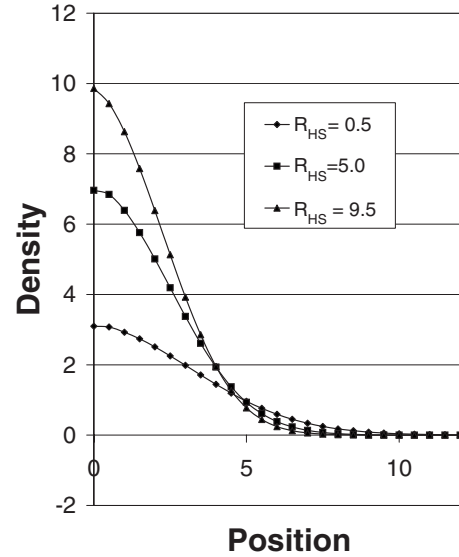


FIG. 2. Density of chain particles as a function of distance from the chain centroid, $g_{\text{pc.m.}}(r)$, for the smallest (0.5 \AA), median (5.0 \AA), and largest (9.5 \AA) values of R_{HS} .

are no repulsive forces between the pseudoparticles comprising the chain, their density near the chain center of mass can become quite large. This can be seen in Fig. 2, a plot of $g_{\text{pc.m.}}(r)$ versus distance from the c.m., where $g_{\text{pc.m.}}(r)$ becomes more peaked around the chain c.m. as the chain becomes more confined within its self-trapped bubble. The maximum value for the case $R_{\text{HS}} = 0.5$ \AA is approximately one-third that of the 9.5 \AA curve; however, it has a much longer nonzero tail than the other curves.

The structural properties of the fluid are the chain-fluid radial distribution function $g_{\text{PF}}(r)$ and the mean local density of fluid atoms about the chain c.m., $g_{\text{fc.m.}}(r)$. These properties can be used to determine the local deformation of the fluid caused by the creation of the self-trapped state. $g_{\text{PF}}(r)$ yields the mean density of fluid atoms at a distance of r from a chain particle, while $g_{\text{fc.m.}}(r)$ provides the same quantity with respect to the chain c.m. As usual, they are normalized to unity in the large- r limit. Figures 3 and 4 are, respectively, plots of $g_{\text{PF}}(r)$ and $g_{\text{fc.m.}}(r)$ vs position. As can be seen in Fig. 3, the larger the value of R_{HS} , the smaller the likelihood that a fluid molecule will be near a pseudoparticle. Because the positronium pick-off decay rate depends upon the number of valence electrons available for annihilation, a consequence is a much smaller value of the decay rate in a self-trapped state as compared to that in an extended state. In the trapped state the positron is shielded from the host atomic electrons by the impenetrable, tightly wound, cluster of pseudoparticles discussed above. Figure 4 shows even more clearly than the previous figure the effect the formation of a self-trapped state has on the fluid. We see the transition from an extended state, with a nonzero value of the fluid density at the origin, to a fully trapped state, where the fluid molecules have been completely excluded from the neighborhood of the chain c.m. Hints of oscillation on large scales, which we are unable to accurately resolve with the present system size, can be seen in both plots. An interesting question is whether these are simply finite size effects, or represent a coupling

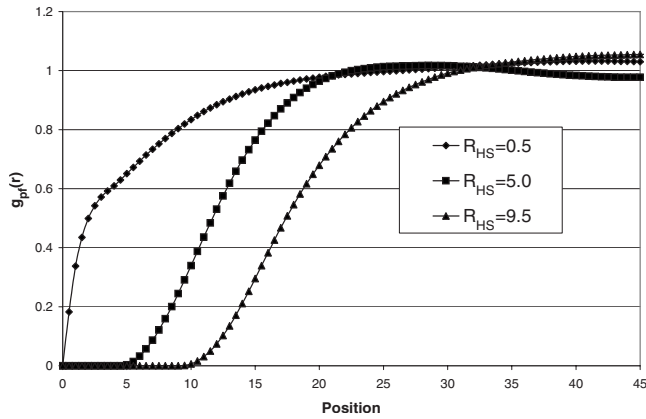


FIG. 3. Scaled density (radial distribution function) of host fluid atoms a distance r from a QP representation (i.e., a time slice or “chain particle”) $g_{PF}(r)$ for three values of R_{HS} .

between the correlation length of the fluid and the thermal (or de Broglie) wavelength of the QP. We will return to this point in Sec. III D.

C. Decay rate

As an added bonus, $g_{fc.m.}(r)$ can be used to compute the number of fluid atoms excluded from the vicinity of the chain. We found that the volume of the fluid atoms excluded from the trapping region is at least twice as great for $R_{HS} = 9.5 \text{ \AA}$ as it is for either 0.5 or 5.0 \AA . Since increases in R_{HS} will lead to decreases in the number of fluid molecule valence electrons around the chain particles available for annihilation, the pick-off decay rate is expected to decrease with increasing R_{HS} . In Fig. 5 we see that the decay rate in our simulations is an exponentially decreasing function of R_{HS} with a characteristic length of 3.71 \AA . Although a realistic estimate of the Ps-atom interaction radius would place it in

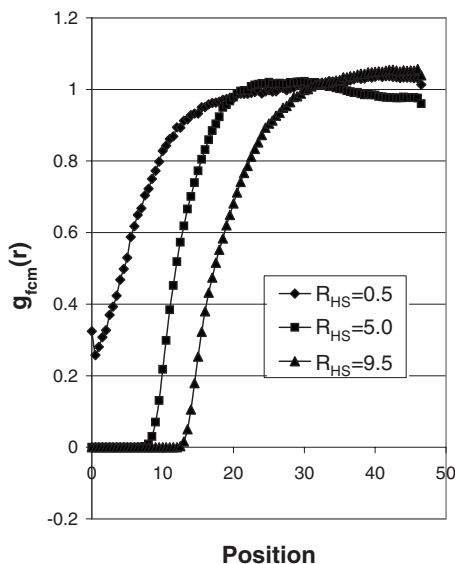


FIG. 4. Scaled density of fluid atoms (radial distribution function) as a function of distance from the chain c.m., $g_{fc.m.}(r)$, for three values of R_{HS} .

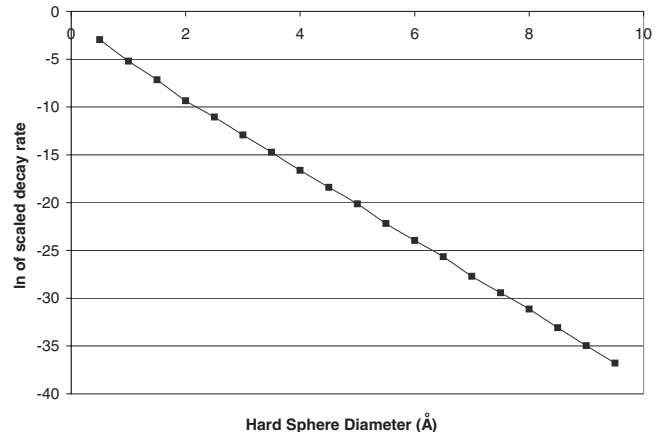


FIG. 5. Natural logarithm of the scaled pick-off decay rate versus R_{HS} .

the interval of 1.0–5.0 \AA , extending the range in the computations clinches the exponential dependence. In our model the Ps atom is treated as a composite particle in its hydrogenic ground state with an exponentially decreasing wave function representing the spread of the positron from the Ps center of mass. This is justified by the small ratio $\approx 4 \times 10^{-3}$ of kT_c to the positronium excitation energy. For simplicity, the electron density associated with each fluid atom is modeled as a δ function. Thus the decay rate is dependent upon both the portion of the positron ground state wave function that manages to leak beyond R_{HS} and the number of fluid atoms centers it overlaps. The exponential decrease in the decay rate with increasing R_{HS} results from the decrease in both the density of fluid atoms and the amplitude of the positron wave function in the shell surrounding the hard sphere surface.

D. Comparison of size effects

In Figs. 3 and 4 the curves seem to oscillate around unity at large distances away from the origin for all three R_{HS} values. At these distances the direct effect from the Ps atom should be minimal. As mentioned earlier, it is possible that these oscillations indicate an interaction between the Ps thermal wavelength and the local fluid density. It is expected that the coupling will be greatest at the critical point because of the large isothermal compressibility. In our previous simulations there was no hint of these oscillations except at the critical density for $T=300 \text{ K}$. It is also possible that the density increases beyond unity in these plots because the system volume is not large enough and the fluid molecules crowd upon each other at the boundary. A possible approach for resolving this conundrum is to compare the g_{PF} and $g_{fc.m.}$ curves for different values of N with correspondingly different system sizes. In both cases we anticipate that the plots would remain the same well below the QP thermal wavelength, i.e., below say 10–15 \AA , while major differences could occur at greater distances. If the latter conjecture is correct, then the maximum of the curves will occur further from the origin with increasing N , indicating that edge effects alone are responsible for the rise in density at large

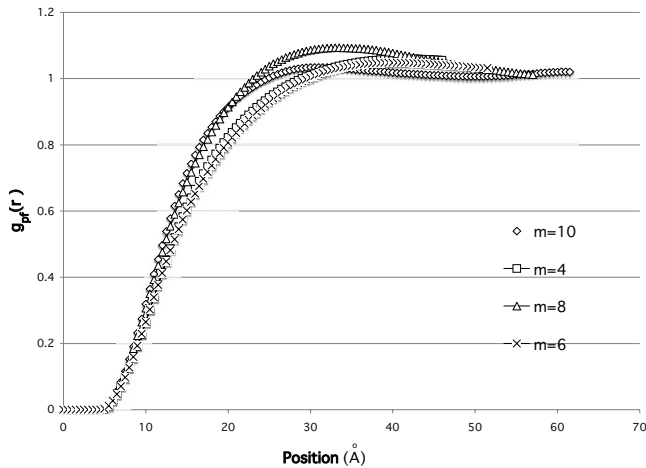


FIG. 6. Radial distribution function g_{PF} versus position for four different values of N (4000, 6000, 8000, and 10 000), showing the evidence of finite-size effects near the critical point.

distances from the Ps atom. On the other hand if the former possibility is correct, while the curves will not lie on top of one another, the maxima of the plots will be near each other. Figure 6 is a plot of g_{PF} for four different values of N for an R_{HS} of 5.0 Å. As shown in the figure, as N is increased, as a result of the larger system size the distance that the curve covers also increases. However, for all curves, the maximum of the first crest occurs at about 30 Å and, for $N=10\,000$, clear oscillations are observed, indicating that they are a real effect and not an artifact of the system size being too small.

IV. CONCLUSIONS

In this work we have employed the path-integral Monte Carlo technique [24] to investigate the equilibrium properties of a generic particle obeying quantum mechanics (QP) interacting with a classical fluid for the interesting case where the fluid is very close to the liquid-vapor critical point. The QP-fluid interaction was modeled by the hard sphere potential and the fluid atoms interacted with each other via a truncated Lennard-Jones 6-12 potential [32]. We have studied both how the presence of the fluid modifies the intrinsic properties of the QP, and the converse, how the QP disrupts the local density of the fluid in its neighborhood. An important focus of the work is the dependence of these local properties on the range of the hard sphere QP-fluid interaction, R_{HS} . In particular, we computed the dependence of the local density of both the QP and the fluid on the distance from the QP center of mass. We also investigated properties directly related to the discretized form of the Feynman-Kac path integral, such as the rms separations between QP positions separated by t time slices on the chain, and the radial distribution of fluid atoms surrounding each of these “pseudoparticle” positions.

A major motivating factor for this study is the fact that the singular isothermal compressibility at the liquid-vapor critical point strongly enhances the ability of a QP to localize in a mesoscopic, reduced density fluctuation. Two noteworthy features that were revealed by this study concern the minimum interaction range for localization, and the long-range

behavior of the QP-atom radial distribution function. In our investigation of the short-range behavior of the fluid atom density in the neighborhood of the QP, we found that, when the hard sphere interaction diameter fell below 1.5 Å, fluid atoms were able to penetrate within the core of the thermalized chain, indicating that self-trapping was no longer complete. This was revealed by the fact that $g_{\text{fc.m.}}(0) > 0$ when $R_{\text{HS}} < 1.5$ Å. Thus, even at the critical point, there is a minimum QP-atom scattering length required for localization.

A result of the divergent correlation length at the critical point is the presence of strong finite-size effects in Monte Carlo and molecular dynamics simulations [45]. To determine their role, we carried out our Monte Carlo simulations for a range of fluid populations such that the system size varied between three and four QP thermal wavelengths. Compared with our earlier simulations at higher temperature [30], here we found visible evidence of QP-induced fluid structure out to $r=70$ Å. For example, the plot of $g_{\text{PF}}(r)$ for $R_{\text{HS}}=5.0$ Å shown in Fig. 6 for a system of 10 000 atoms suggests a slow, decreasing, spatial oscillation with a period on the order of 60–70 Å, much greater than the interatomic spacing or direct interaction ranges. It is highly probable that this remarkable feature is a consequence of the proximity to the critical point of the pure fluid. In addition to the short-range length scales associated with the direct interatomic and QP-atom interactions, and the very long-range interatomic critical point correlation length, the de Broglie wavelength also plays an important role. It is interesting that the slow oscillations observed in the local fluid density are on the order of the de Broglie wavelength at the critical temperature, 87 Å, which may play an enhanced role near the critical point.

An important experimental signature of localization is the reduced positronium pick-off annihilation rate. Some time ago we showed that for an unstable particle, such as a positron or the composite positronium, the annihilation rate could be expressed in terms of the discretized path-integral QP-atom radial distribution function $g_{\text{PF}}(r)$ and the local atomic or molecular electron density [21]. Since the positronium-atom scattering length is typically positive [2], its behavior is dominated by the repulsive core and thus reasonably well represented by the hard sphere interaction employed here. In the present work we took advantage of this connection to show how the annihilation rate at the critical point depends on the range of interaction for a simplified form of the electron distribution. As demonstrated above, the dependence is nearly exponential with a characteristic distance of about 3.7 Å for the model parameters corresponding to the critical point of xenon. Thus the decay rate depends sensitively on the interaction range. This feature may be useful for extracting information concerning the QP-atom interaction from experimental lifetime measurements. It is likely that this sensitivity prevails at other temperatures and densities, but it has not been investigated to date. Two extensions for the future are the introduction of a more realistic atomic electron distribution and a positronium-atom interaction potential that accounts for both dispersion forces and a softer core.

In contrast with mean field models, the power of the PIMC method is that it reveals the complete picture of both the distribution of QP quantum states and the response of the

fluid to the QP “impurity.” In general we have found that, compared with mean field calculations carried out for liquids [5,6], the mesoscopic region in which the QP is localized is much larger at the critical point. Moreover, the density profile of the fluid has a different shape—the “walls” are not nearly as steep and the structure is less sharply defined. Our PIMC calculations for a supercritical fluid at other densities and higher temperatures show similarities with the critical point, but the behavior is less extreme [30]. In particular, rapid oscillations on the scale of the Lennard-Jones distance parameter are clearly articulated in $g_{f.c.m.}(r)$, the radial distribution function of fluid atoms surrounding the pseudoparticle center of mass, at higher density [30]. These all but vanish in the present work. Since the model includes all effects, e.g., the long-range correlation length and the large compressibility near the critical point, it is not possible to unequivocally state which particular fluid feature is responsible for the change in structure, although one is tempted to make conjectures.

The importance of the density of states in understanding self-trapping of quantum particles was pointed out some time ago by Hernandez [3]. In future work we will employ the PIMC technique to directly evaluate the density of states of the QP. We will thus be able to decide when excited states play a role in determining the fluid structure. From the density of states we will also be able to determine the angular distribution of the annihilation photons from positronium, which can be directly compared with experiment. To date this could only be approached from the mean

field theory formulations [7,11,12,15]. It will be interesting to see what changes result from an *ab initio* computation that includes the effects of correlated fluctuations occurring from both quantum statistics and the fluid density.

Although the earth’s weak gravitational field can be ignored in many equilibrium experiments, as the liquid-vapor critical point is approached it induces a density gradient in the vertical direction that, in theory, is singular at the critical point [8]. In practice, at a given temperature near T_c , only a thin layer of the fluid can be considered to be uniform and close to the critical point density. Thus, when experiments are performed very close to the critical point on the earth’s surface, the severe gravitational-induced density gradient imposes an effective size restriction [46,47]. The ideal environment for experimentally exploring self-trapping at the critical point would be provided by microgravity. This would strongly reduce the influence of gravitationally induced size effects on the results, so that the full range of the interatomic correlations would be manifest on the trapping probability. With luck, we will not have to wait overly long for this to occur.

ACKNOWLEDGMENTS

The authors benefited from conversations with John Hopkins and David Ceperley, the support of the TCU center for Technology Resources, and the Southern University High Performance Physics Computing Laboratory.

-
- [1] A. Einstein, *Theory of Brownian Motion* (Methuen, New York, 1926).
 - [2] I. M. Charlton and J. W. Humbertson, *Positron Physics* (Cambridge University Press, New York, 2001).
 - [3] J. Hernandez, *Rev. Mod. Phys.* **63**, 675 (1991).
 - [4] A. F. Borghesani and M. Santini, *Phys. Rev. E* **65**, 056403 (2002).
 - [5] D. Dutta, B. N. Ganguly, D. Gangopadhyay, T. Mukherjee, and B. Dutta-Roy, *Phys. Rev. B* **65**, 094114 (2002).
 - [6] T. Mukherjee, S. K. Das, B. N. Ganguly, and B. Dutta-Roy, *Phys. Rev. B* **57**, 13363 (1998).
 - [7] I. T. Iakubov and A. G. Khrapak, *Rep. Prog. Phys.* **45**, 697 (1982).
 - [8] L. E. Reichl, *A Modern Course in Statistical Physics*, 2nd ed. (Wiley-Interscience, New York, 1998).
 - [9] S. Sharma and S. R. Kaffle, *J. Chem. Phys.* **78**, 6897 (1983).
 - [10] S. C. Sharma, S. R. Kaffle, and J. S. Hart, *Phys. Rev. Lett.* **52**, 2233 (1984).
 - [11] R. A. Ferrell, *Phys. Rev.* **110**, 1355 (1958).
 - [12] M. J. Stott and E. Zaremba, *Phys. Rev. Lett.* **38**, 1493 (1977).
 - [13] R. M. Nieminen, I. Valimaa, M. Manninen, and P. Hautojarvi, *Phys. Rev. A* **21**, 1677 (1980).
 - [14] X. Z. Yan and S. T. Tsai, *Phys. Rev. A* **46**, 4704 (1992).
 - [15] B. N. Miller and T. Reese, *Phys. Rev. A* **39**, 4735 (1989).
 - [16] R. P. Feynman, *Statistical Mechanics* (Addison-Wesley, Reading, MA, 1972).
 - [17] D. Chandler, Y. Singh, and D. M. Richardson, *J. Chem. Phys.* **81**, 1975 (1984).
 - [18] Y. Fan and B. N. Miller, *J. Chem. Phys.* **93**, 4322 (1990).
 - [19] T. Sumi and H. Sekino, *J. Chem. Phys.* **120**, 8157 (2004).
 - [20] D. F. Coker, B. J. Berne, and D. Thirumalai, *J. Chem. Phys.* **86**, 5689 (1987).
 - [21] B. N. Miller and Y. Fan, *Phys. Rev. A* **42**, 2228 (1990).
 - [22] G. J. Martyna, A. Hughes, and M. E. Tuckerman, *J. Chem. Phys.* **110**, 3275 (1999).
 - [23] S. D. Inanov and A. P. Lubartsev, *J. Chem. Phys.* **123**, 034105 (2005).
 - [24] D. M. Ceperley, *Rev. Mod. Phys.* **67**, 279 (1995).
 - [25] C. Chakravarty, *Int. Rev. Phys. Chem.* **16**, 421 (1997).
 - [26] J. Chen and B. N. Miller, *Phys. Rev. B* **49**, 15615 (1994).
 - [27] J. Chen and B. N. Miller, *Phys. Rev. E* **48**, 3667 (1993).
 - [28] J. Chen and B. N. Miller, *J. Chem. Phys.* **100**, 3013 (1994).
 - [29] G. A. Worrell and B. N. Miller, *Phys. Rev. A* **46**, 3380 (1992).
 - [30] T. L. Reese and B. N. Miller, *Phys. Rev. E* **64**, 061201 (2001).
 - [31] T. Sumi and H. Sekino, *Chem. Phys. Lett.* **407**, 294 (2005).
 - [32] N. B. Wilding, *Phys. Rev. E* **52**, 602 (1995).
 - [33] J. M. Caillol, *J. Chem. Phys.* **109**, 4885 (1998).
 - [34] M. Tuomisaari, K. Ryttsola, and P. Hautojarvi, *J. Phys. B* **21**, 3917 (1988).
 - [35] B. N. Miller and T. L. Reese, *Mod. Phys. Lett. B* **20**, 169 (2006).
 - [36] B. N. Miller and T. L. Reese, e-print arXiv:cond-mat/0503630.

- [37] M. Sprik, M. L. Klein, and D. Chandler, *Phys. Rev. B* **31**, 4234 (1985).
- [38] V. A. Antonov, in *Quantum Monte Carlo Methods in Physics and Chemistry*, edited by M. P. Nightingale and C. J. Umrigar, NATO Science Series Vol. 525 (Kluwer, Boston, MA, 1999).
- [39] J. A. Barker, *J. Chem. Phys.* **70**, 2914 (1979).
- [40] P. A. Whitlock and M. H. Kalos, *J. Chem. Phys.* **30**, 361 (1978).
- [41] R. G. Storer, *J. Math. Phys.* **9**, 964 (1968).
- [42] A. D. Klemm and R. G. Storer, *Aust. J. Phys.* **26**, 43 (1973).
- [43] J. Cao and B. J. Berne, *J. Chem. Phys.* **97**, 2382 (1992).
- [44] N. Metropolis, A. W. Rosenbluth, M. N. Rosenbluth, A. H. Teller, and E. Teller, *J. Chem. Phys.* **21**, 1087 (1953).
- [45] K. Binder, in *The Monte Carlo Method in the Physical Sciences*, edited by J. E. Gubernatis, AIP Conf. Proc. No. 690 (AIP, Melville, NY, 2003).
- [46] H. K. Leung and B. N. Miller, *Phys. Rev. A* **12**, 2162 (1975).
- [47] H. K. Leung and B. N. Miller, *Phys. Rev. A* **16**, 406 (1977).